The Effect of Heating Rate on Subsurface AlN Formation in Fe-Al Alloys in N_2-O_2 Atmospheres

JUNE BOTT, HONGBIN YIN, and SEETHARAMAN SRIDHAR

When high Al containing Fe alloys such as TRIP steels are exposed to atmospheres that contain N_2 during re-heating, sub-surface nitrides form and these can be detrimental to mechanical properties. Nitride precipitation can be controlled by minimizing the access of the gaseous atmosphere to the metal surface, which can be achieved by a rapid growth of a continuous and adherent surface scale. This investigation utilizes a Au-image furnace attached to a confocal scanning microscope to simulate the annealing temperature *vs* time while Fe-Al alloys (with Al contents varying from 1 to 8 wt pct) are exposed to a O_2-N_2 atm with 10^{-6} atm O_2. The heating times of 1, 10, and 100 minutes to the isothermal temperature of 1558 K (1285 °C) were used. It was found that fewer sub-surface nitride precipitates formed when the heating time was lowered and when Al content in the samples was increased. In the 8 wt pct samples, no internal nitride precipitates were present regardless of heating time. In the 3 and 5 wt pct samples, internal nitride precipitates were nearly more or less absent at heating times less than 10 minutes. The decrease in internal precipitates was governed by the evolving structure of the external oxide-scale. At low heating rates and/or low Al contents, significant Fe-oxide patches formed and these appeared to allow for ingress of gaseous N_2. For the slow heating rates, ingress could have happened during the longer time spent in lower temperatures where non-protective alumina was present. As Al content in the alloy was increased, the external scale was Al_2O_3 and/or $FeAl_2O_4$ and more continuous and consequently hindered the N_2 from accessing the metal surface. Increasing the Al content in the alloy had the effect of promoting the outward diffusion of Al in the alloy and thereby assisting the formation of the continuous external layer of Al_2O_3 and/or $FeAl_2O_4$.

DOI: 10.1007/s11663-014-0116-x

I. INTRODUCTION

TRANSFORMATION induced plasticity (TRIP) steels are important to the automotive industry as a light-weight, high-strength, and high-ductility structural material. In TRIP steels, aluminum functions to stabilize α-ferrite and to prevent the formation of cementite, which leads to carbon enrichment in the retained γ-austenite phase. This retained austenite produces the TRIP effect by transforming into martensite under strain.[1–3] However, aluminum is highly reactive in both liquid and solid steels and can form internal aluminum nitride and oxide particles which can affect the surface quality of the steel.

Iron-aluminum alloys containing up to 8 wt pct aluminum were examined in previous work.[4,5] Heating conditions in the first study were set to replicate slab reheating during the steelmaking process. A schematic of the steelmaking process is shown in Figure 1. After the molten steel is cast, it undergoes secondary cooling, where the slab is sprayed with water to reduce the temperature. Nitrogen and oxygen are both available from the air, and water vapor also contributes to oxidation. The slab is then cooled to room temperature in air in a slab yard. Before hot rolling processes, the slab must be reheated. This occurs in reheat furnaces in an atmosphere produced by the combustion of natural gas and contains carbon dioxide, water vapor, oxygen, and nitrogen. The primary focus of this and the previous study is on the formation of aluminum nitrides during reheating, but as seen in Figure 1, there are various other opportunities for nitrogen to react with the steel, *e.g.*, during cooling during in the caster and hot-rolling.

If there are sufficient levels of aluminum and nitrogen in solution in the system, they will combine to form aluminum nitride. However, oxide films are known to severely limit the penetration of adsorbed nitrogen into the bulk of the material, since the solubility of nitrogen is low in the oxide.[6] Oxides develop on and below the surface of the material.

In particular, α-alumina is well known to form adherent and protective scales on iron-aluminum alloys.[7–12] Development of protective α-alumina scales is well known to be highly dependent on temperature

JUNE BOTT, Post-Doctoral Researcher, is with the Department of Materials Science & Engineering, Carnegie Mellon University, Pittsburgh, PA 15213. Contact e-mail: jbott@cmu.edu HONGBIN YIN, Lead Engineer, is with the Casting, Process Research, East Chicago Center, ArcelorMittal Global R&D, East Chicago, IN 46321. SEETHARAMAN SRIDHAR, TATA Steel/RAEng Chair, is with the Low Carbon Materials Manufacturing, Warwick Manufacturing Group, International Digital Laboratory, University of Warwick, Coventry CV4 7AL, U.K.

Manuscript submitted July 10, 2013.
Article published online July 11, 2014.

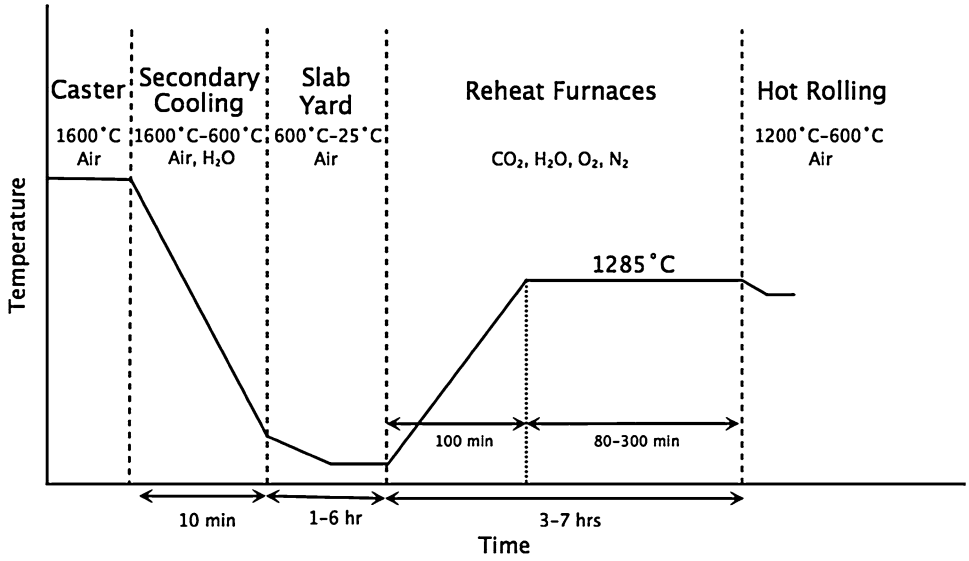

Fig. 1—Temperatures and atmospheres involved in the steelmaking process.

and aluminum content in the alloy.[8,11] For increasing aluminum content, oxidation of Fe-Al alloys will result in scales composed of iron oxide, then mixed iron-aluminum oxides, and finally alumina. For a given temperature, there is a critical aluminum content, below which non-protective oxides form, and above which adherent alumina will develop.

The samples in the previous study were treated in a primarily N_2 atmosphere with oxygen and water vapor impurities. They developed both external oxide scales and internal oxide and nitride precipitates. These subsurface precipitates grew in layers parallel to the sample surface, with oxides in a layer nearer the gas-metal interface and nitrides in a separate layer farther within the sample. It was determined that the composition and morphology of the oxide scale on these samples plays a crucial role in the formation of internal precipitates. Samples with higher aluminum content formed primarily aluminum-based oxides instead of iron-based oxides, and these samples with alumina scales had reduced internal precipitate penetration depths.

In the course of determining the effect of various experimental parameters, it was hypothesized that the initial 100-minute heating period could have an effect on total precipitation depths, so experiments were conducted where the sample was very rapidly heated to temperature. This change in heating rate resulted in samples with entirely different oxide compositions and morphology than the original, slowly heated samples. Increasing the heating rate serves to increase the temperature of the sample during initial scale formation. It was hypothesized that the composition and morphology of the initially formed scale affects all subsequent internal and external oxide and nitride formation, and that the formation of a slow-growing, protective alumina scale would prevent internal precipitate formation.[13]

II. EXPERIMENTS PERFORMED

A. *Experimental Procedure*

Experiments were conducted with various heating rates in a confocal laser-scanning microscope (CLSM), which features a hot stage that focuses infrared radiation from a halogen light bulb onto the sample and crucible to heat the sample, allowing for fine temperature control. Industrial reheating conditions require a slow heating period followed by some isothermal hold. The experiments performed in this study sought to determine the effect of changing that initial heating rate. Samples were heated over the course of 1, 10, or 100 minutes and then held isothermally for an additional 200 minutes to allow for the development of precipitates.

The experiments and the conditions that were varied are listed below in Table I. Alloy compositions are listed in Table II. These experiments were performed in 99.995 pct pure N_2 atmospheres with measured oxygen partial pressure of approximately 10^{-6} atm. The oxygen partial pressure was measured using a zirconia oxygen sensor.

B. *Characterization*

Sample surfaces and cross sections were characterized after heat treatment. X-ray diffraction (XRD) and scanning electron microscopy with energy dispersive X-ray spectroscopy (SEM–EDS) were used to examine the scale and determine the oxide composition and morphology. SEM–EDS was used on sample cross sections to determine the composition and morphology of the scale layers and of the internal precipitates. Precipitate depth was measured from cross-section micrographs for each sample by taking an average of six values.

Table I. Matrix of Heating Rate Experiments

Experiment Name	Alloy Composition (Pct)	Heating Time (min)	Isothermal Time (min)	Isothermal Temperature [K (°C)]
Fe1Al-N2-300	1	100	200	1558 (1285)
Fe1Al-N2-300-10	1	10	200	1558 (1285)
Fe1Al-N2-300-1	1	<1	200	1558 (1285)
Fe3Al-N2-300	3	100	200	1558 (1285)
Fe3Al-N2-300-10	3	10	200	1558 (1285)
Fe3Al-N2-300-1	3	<1	200	1558 (1285)
Fe5Al-N2-300	5	100	200	1558 (1285)
Fe5Al-N2-300-10	5	10	200	1558 (1285)
Fe5Al-N2-300-1	5	<1	200	1558 (1285)
Fe8Al-N2-300	8	100	200	1558 (1285)
Fe8Al-N2-300-10	8	10	200	1558 (1285)
Fe8Al-N2-300-1	8	<1	200	1558 (1285)

Table II. Alloy Compositions

Nominal Aluminum Content (wt pct)	Al (wt pct)	N (ppm)	C (wt pct)	Mn (wt pct)	S (wt pct)	Si (wt pct)
1	1.062	3	0	0	0	0
3	3.002	6	0.152	0.173	0.001	0.011
5	4.886	8	0.149	0.171	0.001	0.016
8	8.044	3	0	0	0	0

III. RESULTS AND DISCUSSION

A. *Surface Oxide Evolution*

CLSM stills of the 1 wt pct aluminum sample are shown below in Figure 2 (100-minute ramp) and Figure 3 (1-minute ramp). Dark oxide patches appear to grow on the 100-minute ramp sample (Figure 2) from inclusions or scratches on the surface at temperatures as low as 623 K (350 °C). As the temperature increases during the initial 100 minutes, the oxide scale grows from these patches into a macroscopically uniform layer.

In the case of the 1-minute ramp, there was not much observable growth on the surface during the heating. The sample was observed to grow darker oxides around inclusions or scratches on the surface during the isothermal hold, similar to the 100-minute sample during the temperature ramp (Figure 2). A layer of lighter-color oxide, presumably alumina, begins to develop around $t = 25$ minutes in Figure 3, and growth of the darker patches slows at this time. It is thought that the alumina covers the rest of the bare iron surface and isolates the iron oxide patches, as is seen in more detail in Figure 4. Further characterization of the alumina scale is discussed later.

The remaining compositions all exhibited similar oxide growth patterns in the CLSM. Oxides grew in patches, which over time mostly coalesced into a uniform oxide. For each composition, decreasing the heating time from 100 to 1 minute causes a change in the structure and composition of the external oxide scale. Scale thickness values and compositions are listed below in Table III. XRD results confirm that the oxide changes from primarily iron-based oxides in the samples heated for 100 minutes to oxides rich in aluminum in the samples heated for 10 and 1 minute.

B. *Internal Precipitation Depth*

SEM micrographs of the cross sections of each 1 wt pct aluminum sample can be found in Figure 5. Figure 5(a) shows the cross-section of the sample after the longest heating time of 100 minutes. The internal precipitate zone consists of: (i) a layer of Al_2O_3-oxides, closest to the interface, (ii) an intermediate layer of AlN- Al_2O_3 dual-phase particles and at further depths, (iii) AlN particles. The structural identification of these particles in the internal precipitation zone was shown in a previous paper.[4] The precipitation of nitrides was shown to occur when the oxygen potential is sufficiently low according to a model presented in literature[14] that assumes that the outer scale is absent or completely permeable to nitrogen. For the 1 wt pct aluminum alloys, as the heating time decreases, the scale changes from a predominantly iron oxide and hercynite scale into a scale with sections of alumina and hercynite. Reducing the heating time to 10 minutes does however not eliminate internal precipitation, as seen in Figure 5(b).

Further reduction of the heating time to 1 minute serves to decrease the amount and distribution of internal precipitation. In Figure 5(c), clusters of internal oxide and nitride precipitates can be seen below the surface of the sample. These clusters are found approximately 500 μm apart and the individual precipitate particles are smaller and are present in smaller quantities than in the slow-heating samples. This cluster phenomenon is distinctly different than the distribution of internal precipitates in the slow heating rate samples. EDS analysis of the scale above each cluster shows that they are covered with iron-rich oxides, where the rest of the surface is covered by aluminum-rich oxides.

In the 3 wt pct aluminum samples, the oxide scale remains predominantly alumina-based, but increasing

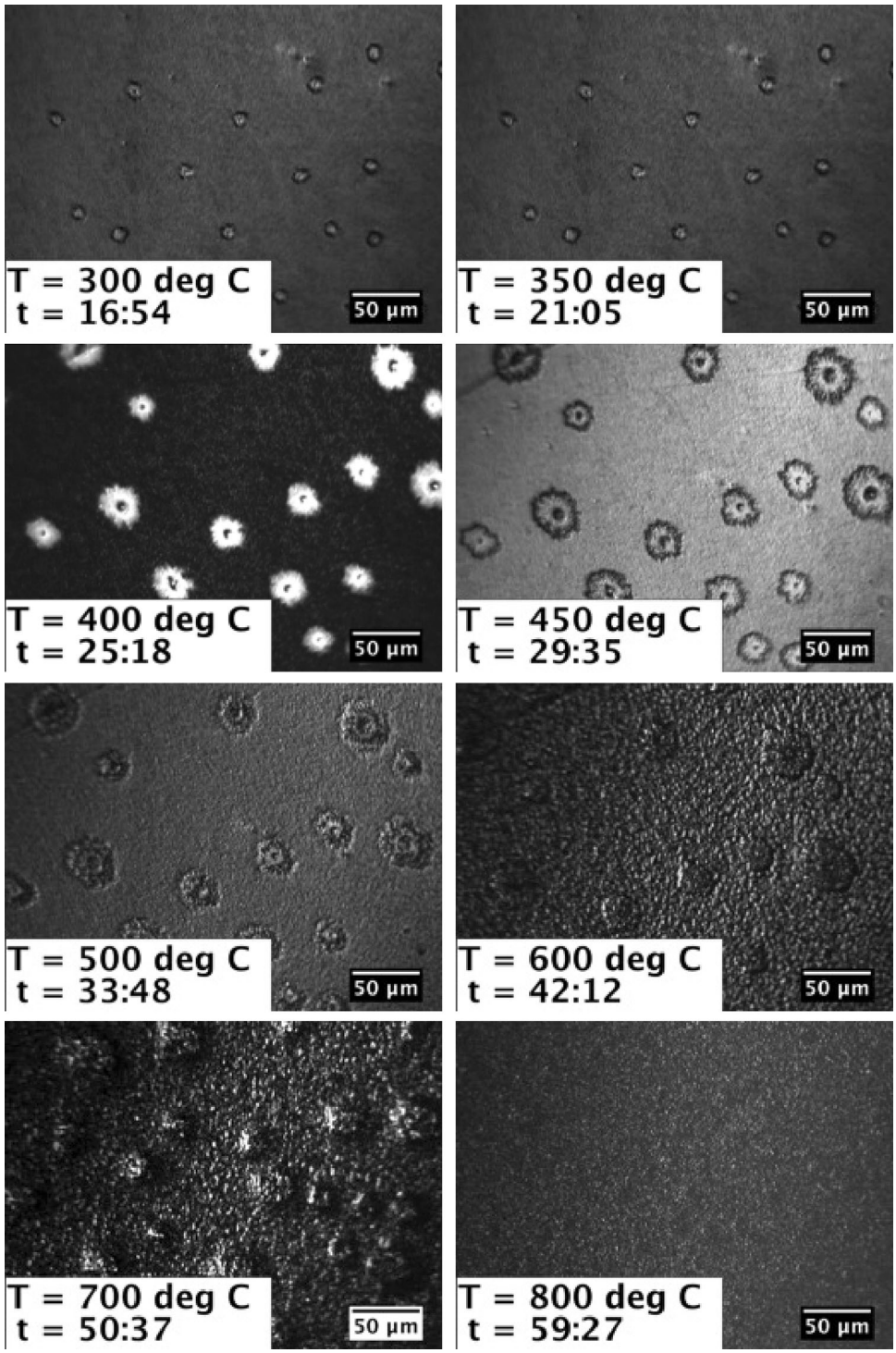

Fig. 2—CLSM images for 1 pct-Al sample. Time is listed in mm:ss.

the heating rate has a larger affect on eliminating internal precipitation, as seen in Figure 6. When the heating time is decreased from 100 to 10 minute, the precipitation depth decreases from 180 μm to 15 μm. Further decreasing the heating time to 1 minute eliminates internal precipitation.

Figure 7 shows that this effect is even more pronounced in the 5 wt pct aluminum alloy. The scale contains less manganese for increasing heating rate, and the improved coverage of the alumina scale eliminates internal precipitation when the heating time is dropped to 10 minutes.

The 8 pct-Al sample exhibited similar changes. The scale changes from a thick iron-oxide rich scale in the slow heating rate sample a 2 μm thick, predominantly alumina scale. Cross sections can be seen in Figure 8.

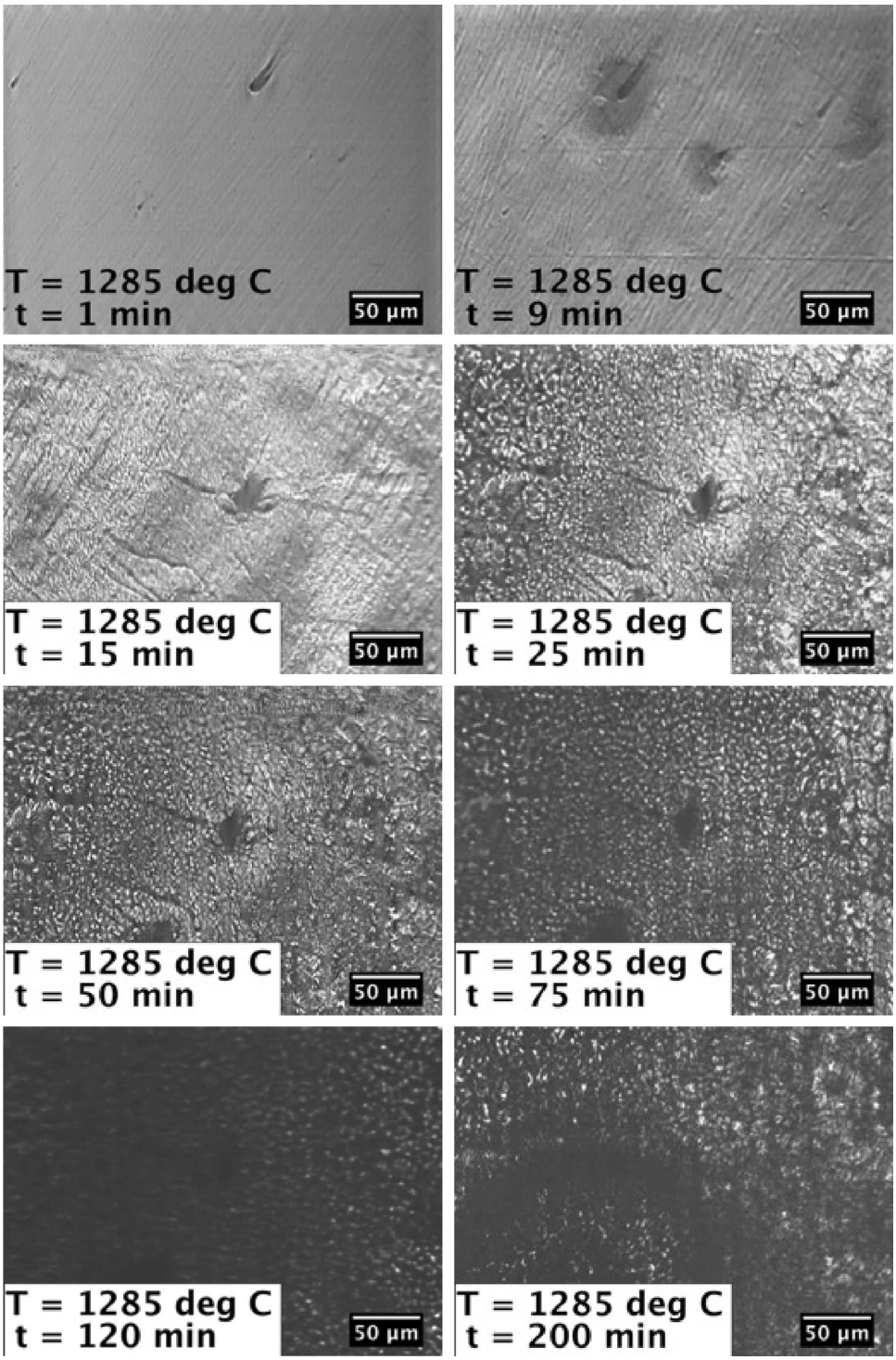

Fig. 3—CLSM images for Fe1Al-N2-300-1. T = 1558 K (1285 °C) for all images.

IV. ANALYSIS

For each composition, the scales that develop on the rapidly heated samples are more aluminum-rich than those that develop on the slowly heated samples (*e.g.*, hercynite or alumina instead of iron oxides). Additionally, for the alloys where the scales are compact and provide complete coverage, the presence of alumina in the scale corresponds with a reduction or elimination of internal precipitation. The internal precipitation depths are shown in Figure 9. Preliminary analysis on the average particle size and quantity in each sample was performed using the Analyze Particles feature of the image processing software ImageJ[15] and is shown in Figure 10.

The average size of particles is shown in Figure 10(a) *vs* the heating time. In the 1 wt pct aluminum samples,

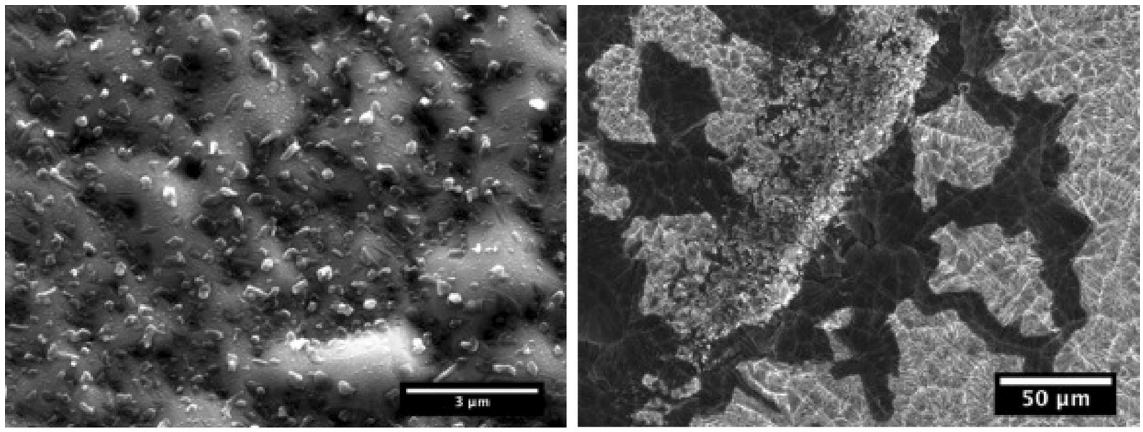

Fig. 4—Surface SEM micrographs of 1 wt pct aluminum heating rate samples. (*a*) 10 min heating time. (*b*) 1 min heating time.

Table III. Scale Compositions and Thicknesses for heating rate experiments

Sample	Scale Composition	Total Scale Thickness (μm)
Fe1Al-N2-300	$FeAl_2O_4$, Fe_3O_4, FeO	1
Fe1Al-N2-300-10	$FeAl_2O_4$	1
Fe1Al-N2-300-1	Al_2O_3, $FeAl_2O_4$	2
Fe3Al-N2-300	Al_2O_3, $MnAl_2O_4$	2
Fe3Al-N2-300-10	Al_2O_3	1
Fe3Al-N2-300-1	Al_2O_3, $MnAl_2O_4$	4
Fe5Al-N2-300	$FeAl_2O_4$, $MnAl_2O_4$	2
Fe5Al-N2-300-10	Al_2O_3	<1
Fe5Al-N2-300-1	Al_2O_3	<1
Fe8Al-N2-300	$FeAl_2O_4$, Fe_3O_4, Al_2O_3	~3
Fe8Al-N2-300-10	Al_2O_3	<1
Fe8Al-N2-300-1	Al_2O_3	2

particle size decreases for increased heating rate. For the 3 and 5 wt pct aluminum samples, the trend is less clear. Because the rapid heating rate largely eliminated internal oxide and nitride formation, the particles that are present likely formed as a result of the initial nitrogen content of the alloys reacting with aluminum. Therefore, precipitate size is less dependent on oxygen and nitrogen diffusion through the surface oxides and more dependent on nucleation and growth processes.

In Figure 10(b), the reduction in the number of internal precipitates for increased heating rate is more prominent as the aluminum content in the samples increases, since a larger bulk concentration of aluminum will increase the driving force for aluminum diffusion to the surface and promote the transition to external oxidation from internal oxidation, as analyzed by Wagner.[16]

The development of a cohesive α-alumina scale has long been known to aid in preventing the formation of internal precipitates and alumina scale grown on iron alloys is well-studied.[7–12] However, the mere presence of alumina in the scale is not enough to eliminate internal precipitation, as seen in the 1 and 3 wt pct aluminum samples. For the 1 pct alloy, though the 1-minute ramp sample has a scale containing both hercynite and alumina, it can be seen in Figure 4(b) that the scale is made up of areas of two different oxides and the alumina is present in patches that are uninterrupted by iron oxides. Therefore, though the alumina provides protection for much of the surface, internal precipitates still develop where iron-based oxides have grown instead.

Even in samples with primarily alumina scales, some internal precipitates can be found, as in the 3 wt pct aluminum 10-minute ramp sample in Figure 6(b). These particles could have formed from oxygen that entered the sample while the alumina developing on the surface had not yet grown into a thick and complete scale, or if the alumina itself was a less protective low-temperature polymorph. γ- and θ-alumina are known to form below 1173 K (900 °C) and form less protective scales than α-alumina.[8,12] The presence of transition alumina polymorphs could not be confirmed, as the isothermal hold at high temperature should allow sufficient time for the transition to the more stable α-alumina.[17]

This study focuses on understanding the mechanism of scale growth at various heating rates. The critical phase of scale growth occurs during the first minutes of heating and the scale that develops in this first phase influences the morphology and composition of the scale throughout the rest of heat treatment. The results of this study imply that several steps occur as the temperature is increased in a given experiment:

1. At low temperatures [starting around 573 K (300 °C)] or low aluminum contents, iron oxides and transition aluminas (*e.g.*, γ- or θ-Al_2O_3) are likely to form, and these oxides can allow the inward diffusion of oxygen and nitrogen.
2. If there is sufficient aluminum at the surface, alumina and/or hercynite can develop. This can occur either at higher aluminum contents or at higher temperatures, which allows for more rapid diffusion of aluminum through the iron matrix.

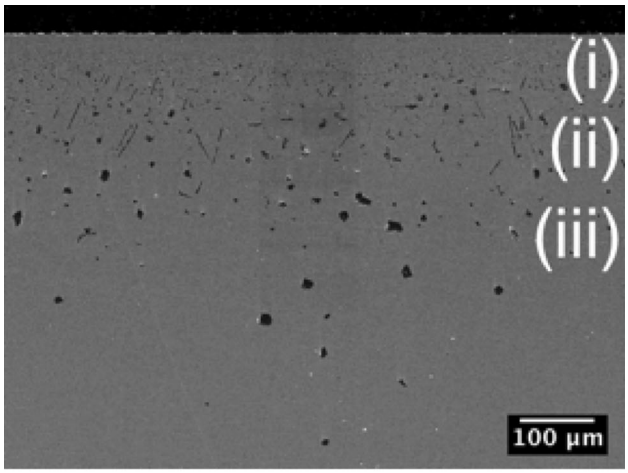

(a) Fe1Al-N2-300

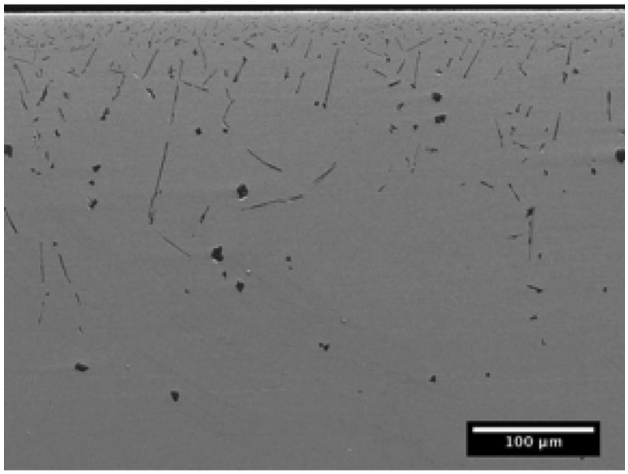

(b) Fe1Al-N2-300-10

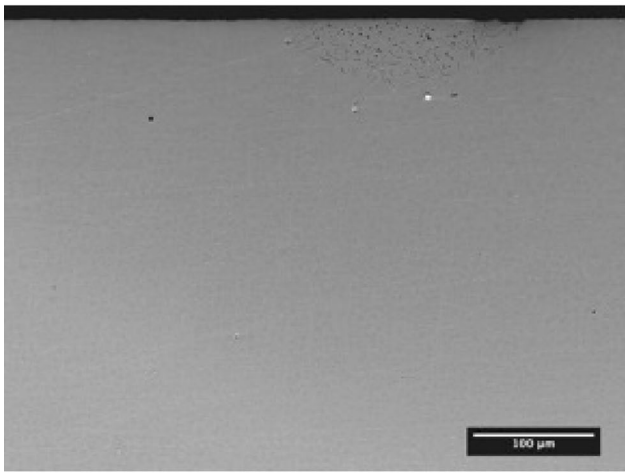

(c) Fe1Al-N2-300-1

Fig. 5—Cross sectional SEM micrographs of 1 wt pct aluminum heating rate samples, where in (a), the internal precipitate layers are as follows: (i) a layer of Al_2O_3-oxides, (ii) an intermediate layer of AlN-Al_2O_3 dual-phase particles, and (iii) AlN particles.

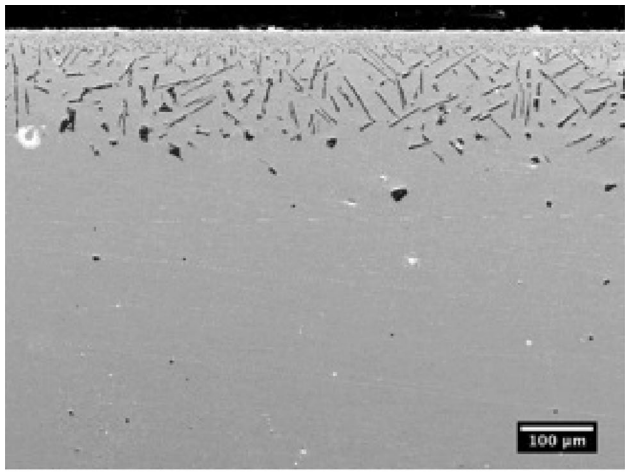

(a) Fe3Al-N2-300

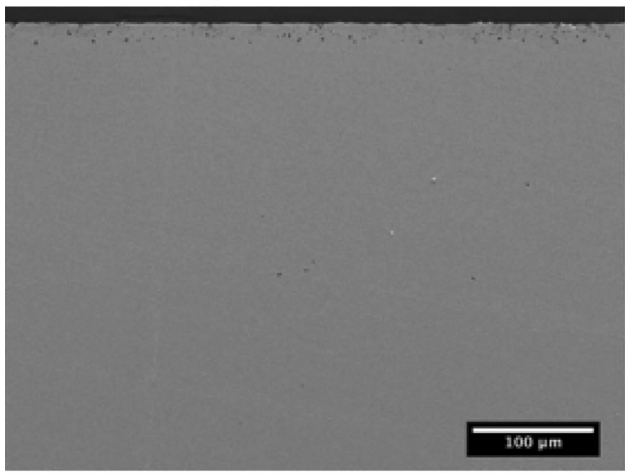

(b) Fe3Al-N2-300-10

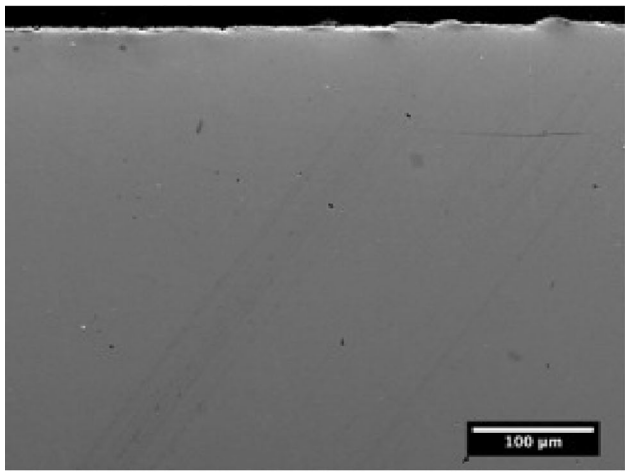

(c) Fe3Al-N2-300-1

Fig. 6—Cross sectional SEM micrographs of 3 wt pct aluminum heating rate samples. (*a*) Fe3Al-N2-300, (*b*) Fe3Al-N2-300-10 (*c*), Fe3Al-N2-300-1.

3. Alumina and/or hercynite formation slows the development of iron oxides as the aluminum-rich oxides begin to cover the bare iron surface.

The formation of iron-oxides in the first step is dependent initially on gas-phase oxygen transport and/or Fe^{2+} migration and both of these processes are

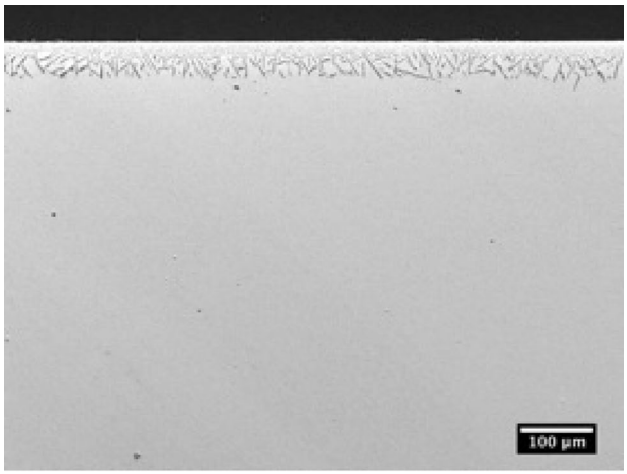

(a) Fe5Al-N2-300

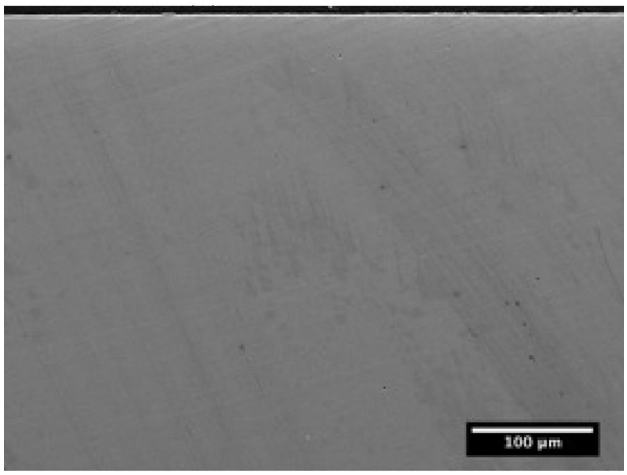

(b) Fe5Al-N2-300-10

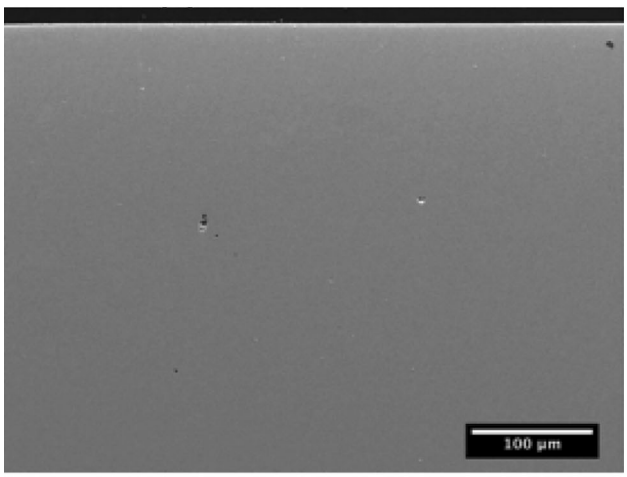

(c) Fe5Al-N2-300-1

Fig. 7—Cross sectional SEM micrographs of 5 wt pct aluminum heating rate samples. (*a*) Fe5Al-N2-300, (*b*) Fe5Al-N2-300-10, (*c*) Fe5Al-N2-300-1.

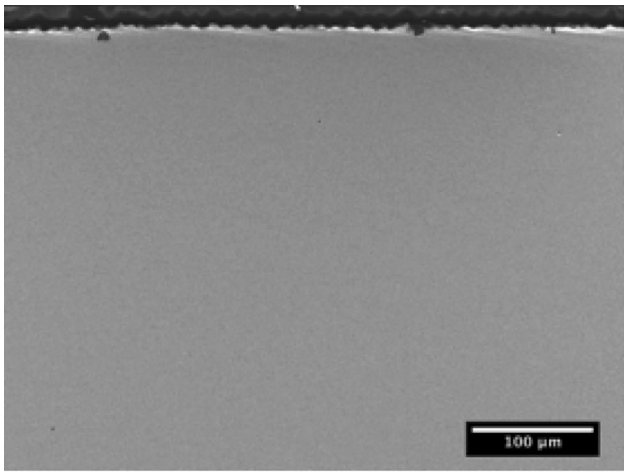

(a) Fe8Al-N2-300

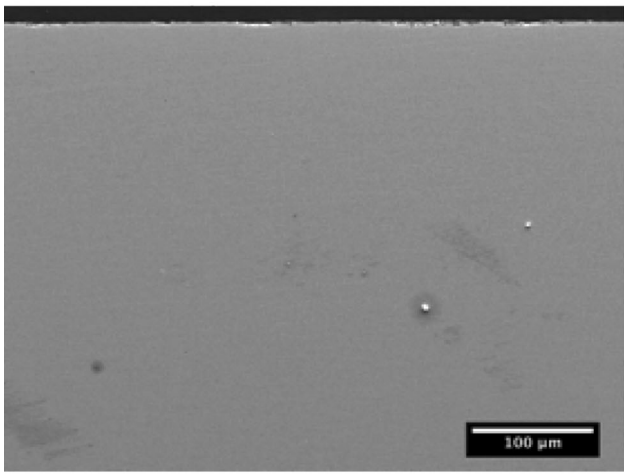

(b) Fe8Al-N2-300-10

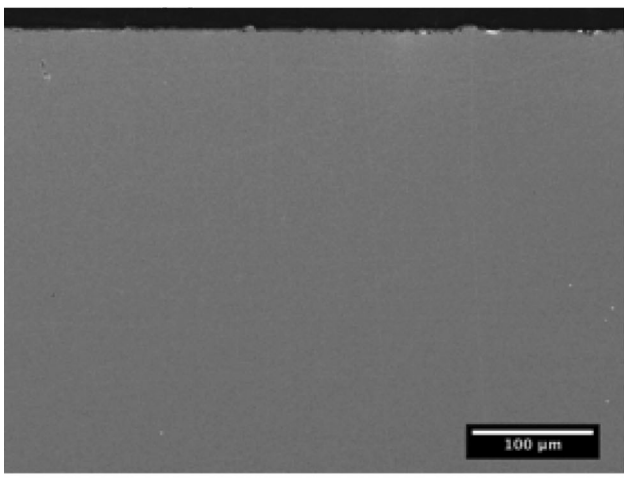

(c) Fe8Al-N2-300-1

Fig. 8—Cross sectional SEM micrographs of 8 wt pct aluminum heating rate samples. (*a*) Fe8Al-N2-300, (*b*) Fe8Al-N2-300-10, (*c*) Fe8Al-N2-300-1.

relatively fast, even at relatively low temperatures.[18] At 1073 K (800 °C), the diffusivity of iron ions through wüstite is approximately 10^{-7} cm^2/s.[19] Alumina growth on the other hand depends on Al diffusion from the bulk alloy to the surface and since alumina is a substitutional element it would be a slow process at lower temperatures.

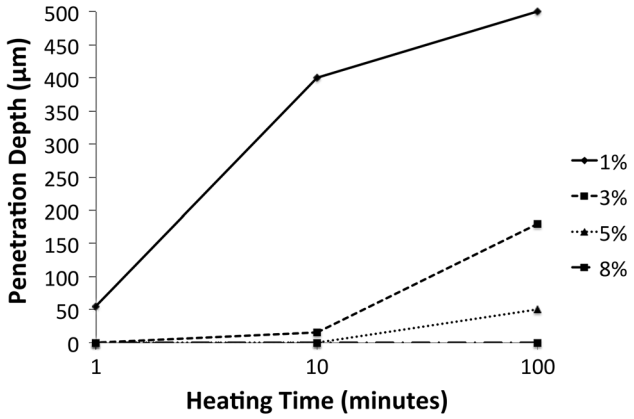

Fig. 9—Heating time *vs* precipitate penetration depth.

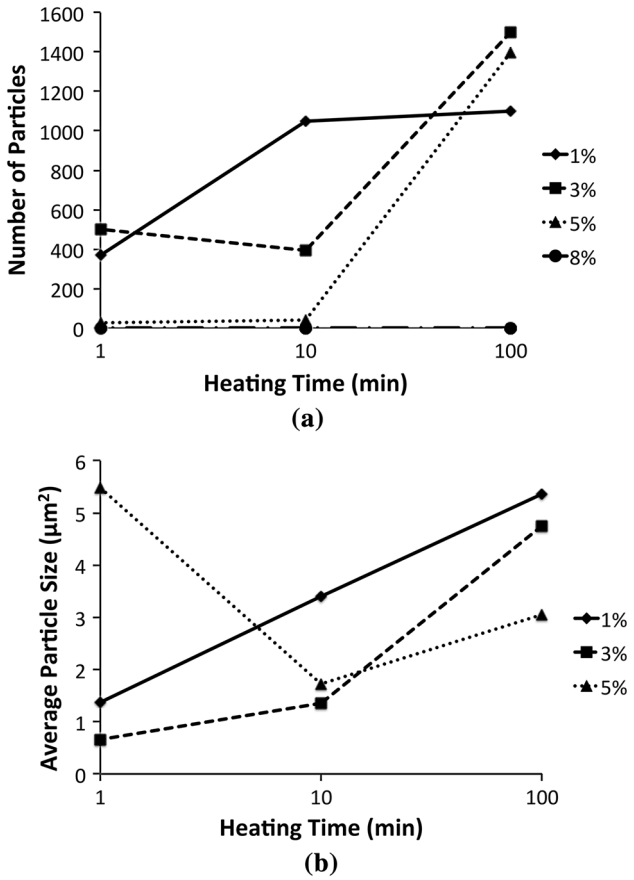

Fig. 10—Graphs of heating time *vs* the number and size of particles developed in 1-, 3-, and 5 pct-aluminum samples. (*a*) Heating time *vs* average particle size for alloys that developed internal precipitates. (*b*) Heating time *vs* the number of particles in alloys that developed internal precipitates.

The diffusivity of aluminum through iron at 1073 K (800 °C) is approximately 10^{-11} cm^2/s, five orders of magnitude smaller than that of iron ions through wüstite.[20]

This first step in the oxide growth process allows for the development of non-protective oxides. The detrimental effects of this step can either be mitigated by increasing the aluminum content, as noted in previous work,[4] or by minimizing the amount of time that the sample spends at lower temperatures. Increasing the temperature rapidly reduces the amount of iron oxides that can nucleate and grow at low temperatures, and at high temperatures, aluminum is more readily available at the gas-metal interface to form alumina. However, there is also a competition between iron and aluminum that becomes evident in alloys with lower aluminum content and can reduce the effectiveness of the protective scale. Though industrial atmospheres are much more oxidizing that those used in these experiments, these results reveal that rapid heating of slab surfaces could potentially modify the scale characteristics and alleviate some internal precipitation problems.

V. CONCLUSIONS

The makeup of the external oxide that develops on iron-aluminum alloys proves to play a large role in internal aluminum nitride formation. Previous work[4] demonstrated that increasing the aluminum content of the alloy causes a shift from iron-based to aluminum-based surface oxides, which are more protective. This study finds that this same shift can be induced by heating the sample rapidly instead of slowly. Longer time spent at lower temperatures where alumina is not protective contributes to the increased nitrogen ingress. The increased temperature during the initial minutes of oxide formation allows for more aluminum to be available as the scale first develops, which results in more protective aluminum-rich oxides.

ACKNOWLEDGMENTS

The authors acknowledge ArcelorMittal Global R&D for their financial support and other in-kind support of this project. They would like to thank E. Mantle at ArcelorMittal Global R&D EC Center for making the lab ingots. The discussions with Drs. O. Lanzi, S. Atreya, and S. Bhat, all at ArcelorMittal Global R&D EC Center, were very valuable in the present study. The authors would also like to thank J. Wolf and N.T. Nuhfer at Carnegie Mellon University for their assistance with characterization methods.

REFERENCES

1. J. Gao and M. Ichikawa: *Proc. Int. Conf. on Advanced High Strength Sheet Steels for Automotive Applications*, Winter Park, CO, June 6–9, 2004, AIST, Warrendale, PA, 2004, pp. 107–15.
2. T.L. Baum, R.J. Fruehan, and S. Sridhar: *Metall. Mater. Trans. B*, 2007, vol. 38B, pp. 287–97.
3. M. De Meyer, D. Vanderschueren, and B.C. De Cooman: *ISIJ Int.*, 1999, vol. 39, pp. 813–22.
4. J. Bott, H. Yin, J. Zhu, and S. Sridhar: *Mater. Corros.*, 2014, vol. 65, pp. 296–304.
5. J. Bott, H. Yin, and S. Sridhar: *AISTech 2013 Proceedings*, Pittsburgh, PA, May 6–9, 2013, AIST, Warrendale, PA, 2013, pp. 1–11.

6. L.S. Darken, R.P. Smith, and E.W. Filer: *Trans. AIME*, 1951, vol. 191, pp. 1174–79.
7. Z.G. Zhang, F. Gesmundo, P.Y. Hou, and Y. Niu: *Corros. Sci.*, 2006, vol. 48, pp. 741–65.
8. R. Prescott and M.J. Graham: *Oxid. Met.*, 1992, vol. 38, pp. 73–87.
9. R. Prescott and M.J. Graham: *Oxid. Met.*, 1992, vol. 38, pp. 233–54.
10. B.A. Pint, J. Leibowitz, and J.H. DeVan: *Oxid. Met.*, 1999, vol. 51, pp. 181–97.
11. P. Tomaszewicz and J.R. Wallwork: *Oxid. Met.*, 1983, vol. 19, pp. 165–85.
12. P. Tomaszewicz and G.R. Wallwork: *Rev. High Temp. Mater.*, 1978, vol. 4, pp. 75–105.
13. H.J. Grabke, M.W. Brumm, and B. Wagemann: in *Oxidation of Intermetallics*, Wiley-VCH Verlag GmbH, Weinheim, 2007, pp. 79–83.
14. J.L. Meijering: *Advances in Materials Research*, Wiley-Interscience, New York, NY, 1971, vol. 5, pp. 1–81.
15. W.S. Rasband: ImageJ: U. S. National Institutes of Health, Bethesda, MD, http://imagej.nih.gov/ij/, 1997–2012. Accessed 25 Nov 2012.
16. C. Wagner: *Z. Elektrochem.*, 1959, vol. 63, pp. 772–82.
17. A. Boumaza, L. Favaro, J. Lédion, G. Sattonnay, J.B. Brubach, P. Berthet, A.M. Huntz, P. Roy, and R. Tétot: *J. Solid State Chem.*, 2009, vol. 182, pp. 1171–76.
18. P. Kofstad: *Nonstoichiometry, Diffusion, and Electrical Conductivity in Binary Metal Oxides*, Robert E. Krieger Publishing Company, Malabar, FL, 1983, p. 229.
19. L. Himmel, R.F. Mehl, and C.E. Birchenall: *Trans. AIME*, 1953, vol. 197, pp. 822–43.
20. I.A. Akimova, V.M. Mironov, and A.V. Pokoyev: *Phys. Met. Metall.*, 1983, vol. 56, pp. 1225–27.